

Soft-gluon corrections in $t\bar{t}W$ production

Nikolaos Kidonakis and Chris Foster

*Department of Physics, Kennesaw State University,
Kennesaw, GA 30144, USA*

Abstract

We study higher-order QCD corrections for the associated production of a top-antitop quark pair and a W boson ($t\bar{t}W$ production) in proton-proton collisions. We calculate approximate NNLO (aNNLO) and approximate N³LO (aN³LO) cross sections, with second-order and third-order soft-gluon corrections added to the exact NLO QCD result, and we also include electroweak (EW) corrections through NLO. We calculate uncertainties from scale dependence, which are reduced at higher orders, and from parton distributions, and we also provide separate results for $t\bar{t}W^+$ and $t\bar{t}W^-$. We compare our results to recent measurements from the LHC, and we find that the aN³LO QCD + NLO EW predictions provide improved agreement with the data. We also calculate differential distributions in top-quark transverse momentum and rapidity and find significant enhancements from the higher-order corrections.

1 Introduction

The cross sections for the production of a top-antitop quark pair in association with a W boson, i.e. $t\bar{t}W$ production, have been measured at the LHC at 7 TeV [1], 8 TeV [2–4], and 13 TeV [5–9] energies. The measurements have become increasingly precise and have been consistently above the theoretical predictions. Therefore, it is crucial to have higher-order results for this process.

The next-to-leading-order (NLO) QCD corrections for this process were calculated in [10, 11] and, including parton showers, in [12, 13], while electroweak corrections were calculated in [14, 15]. Next-to-next-to-leading-order (NNLO) QCD corrections were calculated (though not exact for the finite part of the two-loop virtual corrections) in [16].

An important contribution to the higher-order corrections comes from the emission of soft (i.e. low energy) gluons. These contributions can be calculated at higher orders and formally resummed, and they are numerically dominant in all top-quark processes studied to date since the cross section receives large contributions from soft-gluon emission near partonic threshold because of the large top-quark mass. Soft-gluon resummation [17–19] is well known to be very important for top-antitop pair production [20–23] and single-top production [24–26]. More recently, the resummation formalism has been extended [27] to $2 \rightarrow 3$ processes in single-particle-inclusive kinematics, in particular tqH production [28], $tq\gamma$ production [29], and tqZ production [30], as well as $t\bar{t}\gamma$ production [31]. In all these processes, the soft-gluon corrections are dominant and account for the majority of the complete corrections at NLO. Thus, it can reasonably be expected that they will also be important for $t\bar{t}W$ production. In this paper, we calculate cross sections from soft-gluon resummation using the formalism of [20, 27]. Alternative resummation formalisms for $t\bar{t}W$ production, with different kinematics, namely using the invariant mass of the $t\bar{t}W$ system, have been used in [32–35].

We use the expansions of the resummed cross section to calculate approximate next-to-next-to-leading-order (aNNLO) and approximate next-to-next-to-next-to-leading-order (aN³LO) cross sections and top-quark differential distributions for $t\bar{t}W$ production. The aNNLO results are derived by adding second-order soft-gluon corrections to the complete NLO calculation which includes QCD plus electroweak (EW) corrections. We find consistency between our aNNLO results and those in

Ref. [16] within uncertainties, which shows that the soft-gluon contributions are indeed dominant not only at NLO but also at NNLO. The aN³LO results are derived by further adding third-order soft-gluon corrections to the aNNLO calculation.

In the next section, we describe the soft-gluon resummation formalism for $t\bar{t}W$ partonic processes. In Section 3, we present numerical results for the total cross section through aN³LO QCD + NLO EW. In Section 4, we present results for the top-quark differential distributions in transverse momentum, p_T , and rapidity. We conclude in Section 5.

2 Resummation for $t\bar{t}W$ production

We begin with the soft-gluon resummation formalism for $t\bar{t}W$ production. At leading order (LO), the parton-level processes are $a(p_a) + b(p_b) \rightarrow t(p_t) + \bar{t}(p_{\bar{t}}) + W(p_W)$, with a and b denoting the two incoming partons (quarks and antiquarks), and we define the usual kinematical variables $s = (p_a + p_b)^2$, $t = (p_a - p_t)^2$, and $u = (p_b - p_{\bar{t}})^2$, as well as $s' = (p_t + p_{\bar{t}})^2$, $t' = (p_b - p_{\bar{t}})^2$, and $u' = (p_a - p_{\bar{t}})^2$. If an additional gluon is emitted in the final state, then momentum conservation gives $p_a + p_b = p_t + p_{\bar{t}} + p_W + p_g$ where p_g is the gluon momentum. We denote the top-quark mass by m_t , and we define a threshold variable $s_4 = (p_{\bar{t}} + p_W + p_g)^2 - (p_{\bar{t}} + p_W)^2 = s + t + u - m_t^2 - (p_{\bar{t}} + p_W)^2$ which involves the extra energy from gluon emission and which vanishes as $p_g \rightarrow 0$. The soft-gluon corrections appear in the perturbative series as terms with coefficients multiplying “plus distributions” of logarithms of s_4 , specifically $\ln^k(s_4/m_t^2)/s_4$ where k takes integer values from 0 through $2n - 1$ for the n th order corrections.

Resummation follows from factorization properties of the cross section and renormalization-group evolution. We begin by writing the differential cross section for $t\bar{t}W$ production in proton-proton collisions as a convolution,

$$d\sigma_{pp \rightarrow t\bar{t}W} = \sum_{a,b} \int dx_a dx_b \phi_{a/p}(x_a, \mu_F) \phi_{b/p}(x_b, \mu_F) d\hat{\sigma}_{ab \rightarrow t\bar{t}W}(s_4, \mu_F), \quad (2.1)$$

where μ_F is the factorization scale, $\phi_{a/p}$ and $\phi_{b/p}$ are parton distribution functions (pdf) for parton a and parton b , respectively, in the proton, and $\hat{\sigma}_{ab \rightarrow t\bar{t}W}$ is the partonic cross section which at a given order also depends on the renormalization scale μ_R .

The cross section factorizes if we take Laplace transforms, defined by

$$\tilde{\sigma}_{ab \rightarrow t\bar{t}W}(N) = \int_0^{s_4^{\max}} \frac{ds_4}{s} e^{-Ns_4/s} \hat{\sigma}_{ab \rightarrow t\bar{t}W}(s_4), \quad (2.2)$$

where N is the transform variable. Under transforms, the logarithms of s_4 in the perturbative series turn into logarithms of N which, as we will see, exponentiate. We also define transforms of the pdf via $\tilde{\phi}(N) = \int_0^1 e^{-N(1-x)} \phi(x) dx$. Replacing the colliding protons by partons in Eq. (2.1) [18, 27, 36], we thus have a factorized form in transform space

$$d\tilde{\sigma}_{ab \rightarrow t\bar{t}W}(N) = \tilde{\phi}_{a/a}(N_a, \mu_F) \tilde{\phi}_{b/b}(N_b, \mu_F) d\tilde{\sigma}_{ab \rightarrow t\bar{t}W}(N, \mu_F). \quad (2.3)$$

The cross section can be refactorized [17, 18, 27] in terms of an infrared-safe short-distance hard function, $H_{ab \rightarrow t\bar{t}W}$, and a soft function, $S_{ab \rightarrow t\bar{t}W}$, which describes the emission of noncollinear soft gluons. These hard and soft functions are 2×2 matrices in the color space of the partonic scattering. We have

$$d\tilde{\sigma}_{ab \rightarrow t\bar{t}W}(N) = \tilde{\psi}_{a/a}(N_a, \mu_F) \tilde{\psi}_{b/b}(N_b, \mu_F) \text{tr} \left\{ H_{ab \rightarrow t\bar{t}W}(\alpha_s(\mu_R)) \tilde{S}_{ab \rightarrow t\bar{t}W} \left(\frac{\sqrt{s}}{N\mu_F} \right) \right\}, \quad (2.4)$$

where the functions ψ are distributions for incoming partons at fixed value of momentum and involve collinear emission [17, 18, 27, 36].

Comparing Eqs. (2.3) and (2.4), we find an expression for the hard-scattering partonic cross section in transform space

$$d\tilde{\sigma}_{ab \rightarrow t\bar{t}W}(N, \mu_F) = \frac{\tilde{\psi}_{a/a}(N_a, \mu_F) \tilde{\psi}_{b/b}(N_b, \mu_F)}{\tilde{\phi}_{a/a}(N_a, \mu_F) \tilde{\phi}_{b/b}(N_b, \mu_F)} \text{tr} \left\{ H_{ab \rightarrow t\bar{t}W}(\alpha_s(\mu_R)) \tilde{S}_{ab \rightarrow t\bar{t}W} \left(\frac{\sqrt{s}}{N\mu_F} \right) \right\}. \quad (2.5)$$

The dependence of the soft matrix on the transform variable, N , is resummed via renormalization-group evolution [17, 18]. Thus, $\tilde{S}_{ab \rightarrow t\bar{t}W}$ obeys a renormalization-group equation involving a soft anomalous dimension matrix, $\Gamma_{S_{ab \rightarrow t\bar{t}W}}$, which is calculated from the coefficients of the ultraviolet poles of the eikonal diagrams for the partonic processes [17–20, 27].

The N -space resummed cross section, which resums logarithms of N , is derived from the renormalization-group evolution of the functions $\tilde{S}_{ab \rightarrow t\bar{t}W}$, $\tilde{\psi}_{a/a}$, $\tilde{\psi}_{b/b}$, $\tilde{\phi}_{a/a}$, and $\tilde{\phi}_{b/b}$ in Eq. (2.5), and it is given by

$$\begin{aligned} d\tilde{\sigma}_{ab \rightarrow t\bar{t}W}^{\text{resum}}(N, \mu_F) &= \exp \left[\sum_{i=a,b} E_i(N_i) \right] \exp \left[\sum_{i=a,b} 2 \int_{\mu_F}^{\sqrt{s}} \frac{d\mu}{\mu} \gamma_{i/i}(N_i) \right] \\ &\times \text{tr} \left\{ H_{ab \rightarrow t\bar{t}W}(\alpha_s(\sqrt{s})) \bar{P} \exp \left[\int_{\sqrt{s}}^{\sqrt{s}/N} \frac{d\mu}{\mu} \Gamma_{S_{ab \rightarrow t\bar{t}W}}^\dagger(\alpha_s(\mu)) \right] \right. \\ &\left. \times \tilde{S}_{ab \rightarrow t\bar{t}W} \left(\alpha_s \left(\frac{\sqrt{s}}{N} \right) \right) P \exp \left[\int_{\sqrt{s}}^{\sqrt{s}/N} \frac{d\mu}{\mu} \Gamma_{S_{ab \rightarrow t\bar{t}W}}(\alpha_s(\mu)) \right] \right\}, \quad (2.6) \end{aligned}$$

where P (\bar{P}) denotes path-ordering in the same (reverse) sense as the integration variable μ . The first exponential in Eq. (2.6) resums soft and collinear emission from the initial-state partons [36], while the second exponential involves the parton anomalous dimensions $\gamma_{i/i}$ and the factorization scale μ_F . These are followed by exponentials with the soft anomalous dimension matrix $\Gamma_{S_{ab \rightarrow t\bar{t}W}}$ and its Hermitian adjoint. Explicit results for the first two exponents of Eq. (2.6) can be found in Ref. [27].

The soft anomalous dimensions for $t\bar{t}W$ production are essentially the same as those for the $q\bar{q}$ channel in $t\bar{t}$ production [17, 18, 20, 37], since the color structure of the hard scattering is the same, with only some modifications to account for the $2 \rightarrow 3$ kinematics (see Ref. [38] for a review). For the processes $q(p_a) + \bar{q}'(p_b) \rightarrow t(p_t) + \bar{t}(p_{\bar{t}}) + W(p_W)$ we choose a color tensor basis of s -channel singlet and octet exchange, $c_1^{q\bar{q}' \rightarrow t\bar{t}W} = \delta_{ab}\delta_{12}$, $c_2^{q\bar{q}' \rightarrow t\bar{t}W} = T_{ba}^c T_{12}^c$, where T^c are the generators of SU(3) in the fundamental representation with color indices 1 and 2 for the top and antitop quarks, respectively. Then, the four matrix elements of $\Gamma_{S_{q\bar{q}' \rightarrow t\bar{t}W}}$ are given at one loop [38] by

$$\begin{aligned} \Gamma_{11}^{(1)}{}_{q\bar{q}' \rightarrow t\bar{t}W} &= \Gamma_{\text{cusp}}^{(1)}, \quad \Gamma_{12}^{(1)}{}_{q\bar{q}' \rightarrow t\bar{t}W} = \frac{C_F}{2N_c} \Gamma_{21}^{(1)}{}_{q\bar{q}' \rightarrow t\bar{t}W}, \quad \Gamma_{21}^{(1)}{}_{q\bar{q}' \rightarrow t\bar{t}W} = \ln \left(\frac{(t - m_t^2)(t' - m_t^2)}{(u - m_t^2)(u' - m_t^2)} \right), \\ \Gamma_{22}^{(1)}{}_{q\bar{q}' \rightarrow t\bar{t}W} &= \left(1 - \frac{C_A}{2C_F} \right) \left[\Gamma_{\text{cusp}}^{(1)} + 2C_F \ln \left(\frac{(t - m_t^2)(t' - m_t^2)}{(u - m_t^2)(u' - m_t^2)} \right) \right] + \frac{C_A}{2} \left[\ln \left(\frac{(t - m_t^2)(t' - m_t^2)}{s m_t^2} \right) - 1 \right] \end{aligned} \quad (2.7)$$

where $\Gamma_{\text{cusp}}^{(1)} = -C_F(L_{\beta_t} + 1)$ is the one-loop QCD massive cusp anomalous dimension, with $L_{\beta_t} = (1 + \beta_t^2)/(2\beta_t) \ln[(1 - \beta_t)/(1 + \beta_t)]$ and $\beta_t = \sqrt{1 - 4m_t^2/s'}$. Also, $C_F = (N_c^2 - 1)/(2N_c)$ and $C_A = N_c$, where $N_c = 3$ in QCD.

At two loops, we have

$$\begin{aligned}\Gamma_{11\,q\bar{q}'\rightarrow t\bar{t}W}^{(2)} &= \Gamma_{\text{cusp}}^{(2)}, \quad \Gamma_{12\,q\bar{q}'\rightarrow t\bar{t}W}^{(2)} = \left(K_2 - C_A N_2^{\beta_t}\right) \Gamma_{12\,q\bar{q}'\rightarrow t\bar{t}W}^{(1)}, \quad \Gamma_{21\,q\bar{q}'\rightarrow t\bar{t}W}^{(2)} = \left(K_2 + C_A N_2^{\beta_t}\right) \Gamma_{21\,q\bar{q}'\rightarrow t\bar{t}W}^{(1)}, \\ \Gamma_{22\,q\bar{q}'\rightarrow t\bar{t}W}^{(2)} &= K_2 \Gamma_{22\,q\bar{q}'\rightarrow t\bar{t}W}^{(1)} + \left(1 - \frac{C_A}{2C_F}\right) \left(\Gamma_{\text{cusp}}^{(2)} - K_2 \Gamma_{\text{cusp}}^{(1)}\right) + \frac{1}{4}C_A^2(1 - \zeta_3),\end{aligned}\quad (2.8)$$

where $K_2 = C_A(67/36 - \zeta_2/2) - 5n_f/18$ with n_f the number of light-quark flavors,

$$N_2^{\beta_t} = \frac{1}{4} \ln^2 \left(\frac{1 - \beta_t}{1 + \beta_t} \right) + \frac{(1 + \beta_t^2)}{8\beta_t} \left[\zeta_2 - \ln^2 \left(\frac{1 - \beta_t}{1 + \beta_t} \right) - \text{Li}_2 \left(\frac{4\beta_t}{(1 + \beta_t)^2} \right) \right], \quad (2.9)$$

and

$$\begin{aligned}\Gamma_{\text{cusp}}^{(2)} &= K_2 \Gamma_{\text{cusp}}^{(1)} + C_F C_A \left\{ \frac{1}{2} + \frac{\zeta_2}{2} + \frac{1}{2} \ln^2 \left(\frac{1 - \beta_t}{1 + \beta_t} \right) \right. \\ &\quad + \frac{(1 + \beta_t^2)}{4\beta_t} \left[\zeta_2 \ln \left(\frac{1 - \beta_t}{1 + \beta_t} \right) - \ln^2 \left(\frac{1 - \beta_t}{1 + \beta_t} \right) + \frac{1}{3} \ln^3 \left(\frac{1 - \beta_t}{1 + \beta_t} \right) - \text{Li}_2 \left(\frac{4\beta_t}{(1 + \beta_t)^2} \right) \right] \\ &\quad + \frac{(1 + \beta_t^2)^2}{8\beta_t^2} \left[-\zeta_3 - \zeta_2 \ln \left(\frac{1 - \beta_t}{1 + \beta_t} \right) - \frac{1}{3} \ln^3 \left(\frac{1 - \beta_t}{1 + \beta_t} \right) - \ln \left(\frac{1 - \beta_t}{1 + \beta_t} \right) \text{Li}_2 \left(\frac{(1 - \beta_t)^2}{(1 + \beta_t)^2} \right) \right. \\ &\quad \left. \left. + \text{Li}_3 \left(\frac{(1 - \beta_t)^2}{(1 + \beta_t)^2} \right) \right] \right\}\end{aligned}\quad (2.10)$$

is the two-loop massive cusp anomalous dimension in QCD [19, 39].

We can expand the resummed cross section, Eq. (2.6), to any fixed order, and then do a straightforward inversion back to momentum space without requiring a prescription [20–22, 27]. Thus, by expanding to N³LO, we can calculate the first-order, second-order, and third-order soft-gluon corrections to the $t\bar{t}W$ production total cross section as well as the top-quark differential distributions. By adding the second-order soft-gluon corrections to the exact NLO results we derive aNNLO predictions, and by further adding the third-order soft-gluon corrections to the aNNLO results we derive aN³LO predictions.

3 Total cross sections

In this section we present results for total cross sections for $t\bar{t}W$ production. We use a top-quark mass $m_t = 172.5$ GeV and set the factorization and renormalization scales equal to each other, with this common scale denoted by μ . The complete NLO results, which include both QCD and EW corrections, are calculated using MADGRAPH5_AMC@NLO [40, 41]. We add second-order soft-gluon corrections to the NLO QCD and NLO QCD+EW results to derive aNNLO QCD and aNNLO QCD + NLO EW cross sections, respectively. We further add third-order soft-gluon corrections to the aNNLO QCD and aNNLO QCD + NLO EW results to derive, respectively, aN³LO QCD and aN³LO QCD + NLO EW cross sections. We use MSHT20 NNLO pdf [42] in our calculations.

In Fig. 1 we display the $t\bar{t}W$ cross sections in proton-proton collisions for LHC energies from 7 to 14 TeV. The plot on the left shows results at LO QCD, LO QCD+EW, NLO QCD, NLO QCD+EW, aNNLO QCD, aNNLO QCD + NLO EW, aN³LO QCD, and aN³LO QCD + NLO EW. The inset plot displays the K -factors, i.e. the ratios of the higher-order results to the LO QCD cross section. It is clear that the NLO QCD corrections are large and the further enhancements from soft-gluon emission at aNNLO and aN³LO are quite significant. The NLO electroweak corrections are also significant.

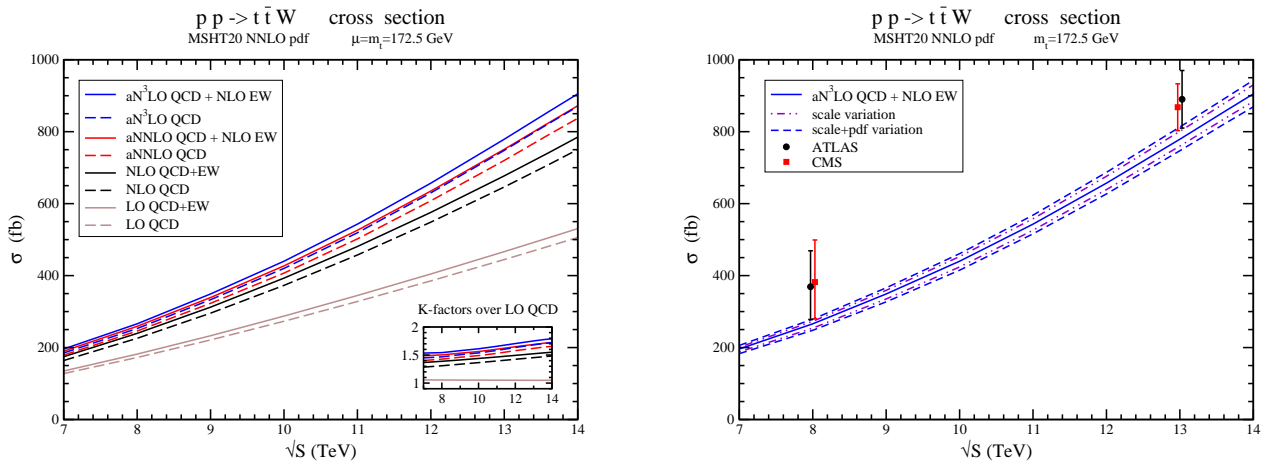


Figure 1: The total cross sections at various orders through aN³LO QCD + NLO EW for $t\bar{t}W$ production in pp collisions at LHC energies using MSHT20 NNLO pdf. The inset in the left plot displays the K -factors relative to LO QCD while the plot on the right shows a comparison with LHC data at 8 TeV [3, 4] and 13 TeV [8, 9] energies.

The plot on the right in Fig. 1 compares the aN³LO QCD + NLO EW theoretical prediction with data from ATLAS and CMS at 8 and 13 TeV energies [3, 4, 8, 9]. In addition to the central result for the theoretical prediction, we also show the scale variation over the interval from $m_t/2$ to $2m_t$ as well as the combined scale and pdf variation. The theoretical results agree with the data within the theoretical and experimental uncertainties.

$t\bar{t}W$ cross sections in pp collisions at the LHC					
σ in fb	7 TeV	8 TeV	13 TeV	13.6 TeV	14 TeV
LO QCD	128^{+39}_{-28}	172^{+51}_{-36}	445^{+114}_{-84}	481^{+121}_{-90}	506^{+126}_{-94}
LO QCD+EW	135^{+41}_{-29}	182^{+53}_{-38}	467^{+119}_{-88}	505^{+127}_{-94}	531^{+132}_{-98}
NLO QCD	164^{+13}_{-17}	226^{+20}_{-23}	646^{+83}_{-74}	708^{+94}_{-82}	750^{+101}_{-88}
NLO QCD+EW	175^{+12}_{-17}	239^{+19}_{-23}	677^{+80}_{-74}	741^{+90}_{-82}	785^{+97}_{-88}
aNNLO QCD	179^{+6}_{-10}	246^{+9}_{-15}	720^{+29}_{-43}	791^{+32}_{-47}	837^{+34}_{-50}
aNNLO QCD + NLO EW	190^{+6}_{-10}	259^{+9}_{-15}	751^{+27}_{-43}	824^{+29}_{-47}	872^{+31}_{-50}
aN ³ LO QCD	185^{+5}_{-8}	253^{+7}_{-12}	748^{+24}_{-19}	822^{+26}_{-20}	870^{+28}_{-21}
aN ³ LO QCD + NLO EW	196^{+5}_{-8}	266^{+7}_{-12}	779^{+22}_{-19}	855^{+23}_{-20}	905^{+25}_{-21}

Table 1: The $t\bar{t}W$ cross sections (in fb) at various orders through aN³LO QCD + NLO EW with scale uncertainties, in pp collisions with $\sqrt{S} = 7, 8, 13, 13.6,$ and 14 TeV, $m_t = 172.5$ GeV, and MSHT20 NNLO pdf.

In Table 1 we show detailed results for the LO QCD, LO QCD+EW, NLO QCD, NLO QCD+EW, aNNLO QCD, aNNLO QCD + NLO EW, aN³LO QCD, and aN³LO QCD + NLO EW cross sections for $t\bar{t}W$ production in pp collisions at LHC energies of 7, 8, 13, 13.6, and 14 TeV. The central results are with $\mu = m_t = 172.5$ GeV, and the scale uncertainty from variation over the interval $m_t/2$ to $2m_t$ is also shown. As expected, the scale uncertainty decreases with increasing pertur-

bative order. At the current LHC energy of 13.6 TeV, the NLO QCD corrections increase the LO QCD result by around 47%, the aNNLO corrections provide another 17% increase, and the aN³LO corrections provide an extra 6% increase. The contribution of the electroweak corrections through NLO is around 7%, similar in size to the aN³LO QCD corrections. The final aN³LO QCD + NLO EW cross section is around 78% bigger than the LO QCD result.

$t\bar{t}W^+$ and $t\bar{t}W^-$ cross sections in pp collisions at the LHC				
σ in fb	$t\bar{t}W^+$ 13 TeV	$t\bar{t}W^+$ 13.6 TeV	$t\bar{t}W^-$ 13 TeV	$t\bar{t}W^-$ 13.6 TeV
LO QCD	299^{+77}_{-57}	322^{+82}_{-60}	146^{+37}_{-28}	159^{+40}_{-30}
LO QCD+EW	313^{+80}_{-59}	337^{+85}_{-63}	154^{+39}_{-29}	168^{+42}_{-31}
NLO QCD	431^{+54}_{-49}	470^{+61}_{-54}	215^{+29}_{-25}	238^{+33}_{-28}
NLO QCD+EW	450^{+51}_{-48}	490^{+58}_{-53}	227^{+28}_{-25}	251^{+32}_{-28}
aNNLO QCD	480^{+19}_{-28}	525^{+21}_{-31}	240^{+10}_{-15}	266^{+11}_{-16}
aNNLO QCD + NLO EW	499^{+17}_{-28}	545^{+19}_{-31}	252^{+10}_{-15}	279^{+10}_{-16}
aN ³ LO QCD	498^{+16}_{-12}	545^{+17}_{-13}	250^{+8}_{-7}	277^{+9}_{-7}
aN ³ LO QCD + NLO EW	517^{+14}_{-12}	565^{+15}_{-13}	262^{+8}_{-7}	290^{+8}_{-7}

Table 2: The separate $t\bar{t}W^+$ and $t\bar{t}W^-$ cross sections (in fb) at various orders through aN³LO QCD + NLO EW with scale uncertainties, in pp collisions with $\sqrt{S} = 13$ and 13.6 TeV, $m_t = 172.5$ GeV, and MSHT20 NNLO pdf.

In Table 2 we show corresponding results separately for the cross sections for $t\bar{t}W^+$ and $t\bar{t}W^-$ production in pp collisions at LHC energies of 13 and 13.6 TeV. The central results are with $\mu = m_t = 172.5$ GeV, and the scale uncertainty from variation over the interval $m_t/2$ to $2m_t$ is also shown. Again, the scale uncertainties decrease with increasing perturbative order. The $t\bar{t}W^+$ cross sections are roughly twice as big as those for $t\bar{t}W^-$. We also find that the higher-order corrections are slightly bigger for the $t\bar{t}W^-$ process than for $t\bar{t}W^+$.

We also want to note that our results are consistent with those in [16] through NNLO QCD + NLO EW, within the uncertainties provided, if we use their choices for the central scale and pdf. This again shows that the soft-gluon contributions are dominant in the higher-order corrections.

Next, we compare our results with data from the LHC at 8 and 13 TeV. We note that the data at both energies are consistently higher than the NLO cross sections. At 8 TeV, CMS has measured a $t\bar{t}W$ production cross section of 382^{+117}_{-102} fb [4] while ATLAS finds 369^{+100}_{-91} fb [3]. Both of these numbers are substantially above the NLO cross sections and even the aNNLO cross sections, and thus we need aN³LO corrections for theory to describe the data. The aN³LO QCD + NLO EW result is $266^{+7}_{-12}{}^{+6}_{-6}$ fb, where the first uncertainty is from scale variation and the second is from the pdf, and this is in good agreement with both the CMS and the ATLAS data.

CMS has recently measured a $t\bar{t}W$ production cross section at 13 TeV of 868 ± 65 fb [8]. Separate measurements were also made for $t\bar{t}W^+$ of 553 ± 42 fb and for $t\bar{t}W^-$ of 343 ± 36 fb [8]. ATLAS has measured a cross section at 13 TeV of 890 ± 80 fb [9]. All of these numbers are substantially above the NLO cross sections and even the aNNLO cross sections, and thus we again need aN³LO corrections to reach agreement with theory. The aN³LO QCD + NLO EW result is $779^{+22}_{-19}{}^{+12}_{-13}$ fb, where the first uncertainty is from scale variation and the second is from the pdf, and this is in good agreement with both the CMS and the ATLAS data. In addition, the aN³LO QCD + NLO EW result for $t\bar{t}W^+$ is $517^{+14}_{-12}{}^{+8}_{-9}$ fb, in good agreement with the CMS data, while for $t\bar{t}W^-$ it is $262^{+8}_{-7}{}^{+4}_{-4}$ fb, bringing the theoretical prediction closer to the data.

4 Top-quark p_T and rapidity distributions

In this section we present results for the top-quark p_T and rapidity distributions in $t\bar{t}W$ production. As for the total cross sections, we use a top-quark mass $m_t = 172.5$ GeV and set the factorization and renormalization scales equal to each other, with this common scale denoted by μ . Again, the complete NLO results include both QCD and EW corrections and are calculated using MADGRAPH5_AMC@NLO [40, 41]. We add second-order soft-gluon corrections to the NLO QCD and NLO QCD+EW results to derive aNNLO QCD and aNNLO QCD + NLO EW distributions, respectively; and we further add third-order soft-gluon corrections to the aNNLO QCD and aNNLO QCD + NLO EW results to derive aN³LO QCD and aNNLO QCD + NLO EW distributions, respectively. Again, we use MSHT20 NNLO pdf [42] in our calculations.

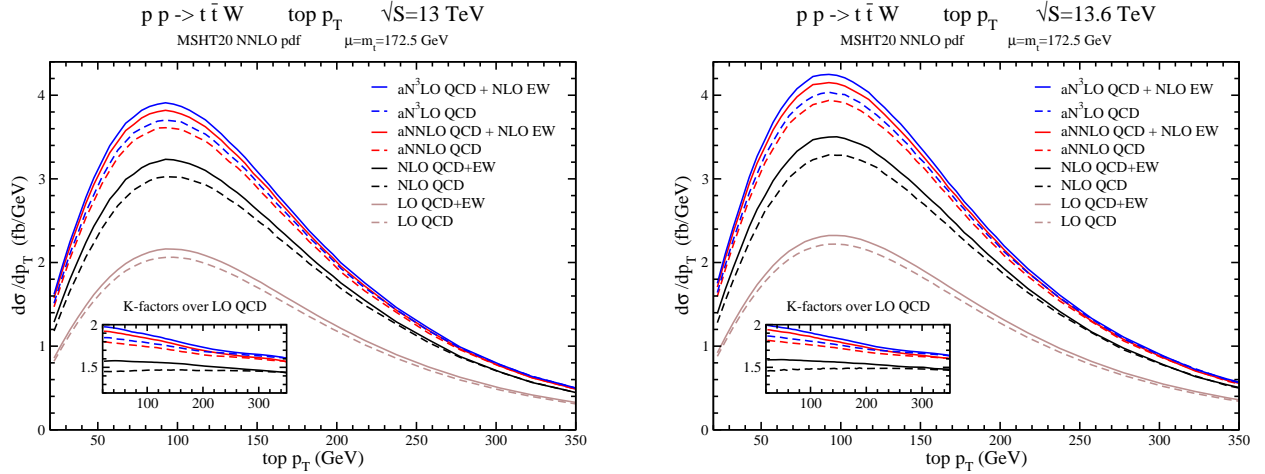


Figure 2: The top-quark p_T distributions at various orders through aN³LO QCD + NLO EW in $t\bar{t}W$ production in pp collisions at LHC energies of 13 TeV (left plot) and 13.6 TeV (right plot) using MSHT20 NNLO pdf. The inset plots display the K -factors relative to LO QCD.

In Fig. 2 we plot the top-quark transverse-momentum distributions, $d\sigma/dp_T$, in $t\bar{t}W$ production at LHC energies of 13 TeV (left plot) and 13.6 TeV (right plot). Results are shown at various orders through aN³LO QCD + NLO EW. The inset plot displays the K -factors, i.e. the ratios of the higher-order results to the LO QCD p_T distribution. As for the total cross section, we see large enhancements in the p_T distribution from the NLO QCD corrections and further significant increases from the higher-order soft-gluon corrections as well as the electroweak corrections. However, the relative sizes of these enhancements change with the value of the top-quark p_T .

In Fig. 3 we plot the top-quark rapidity distributions, $d\sigma/dY$, in $t\bar{t}W$ production at LHC energies of 13 TeV (left plot) and 13.6 TeV (right plot). Results are shown at various orders through aN³LO QCD + NLO EW. The inset plot displays the K -factors, i.e. the ratios of the higher-order results to the LO QCD rapidity distribution. Again, the contributions from the higher-order QCD corrections through aN³LO are large, and the EW corrections are significant. The relative sizes of the enhancements from the higher-order corrections depend on the value of the top-quark rapidity and grow faster at very large rapidity values.

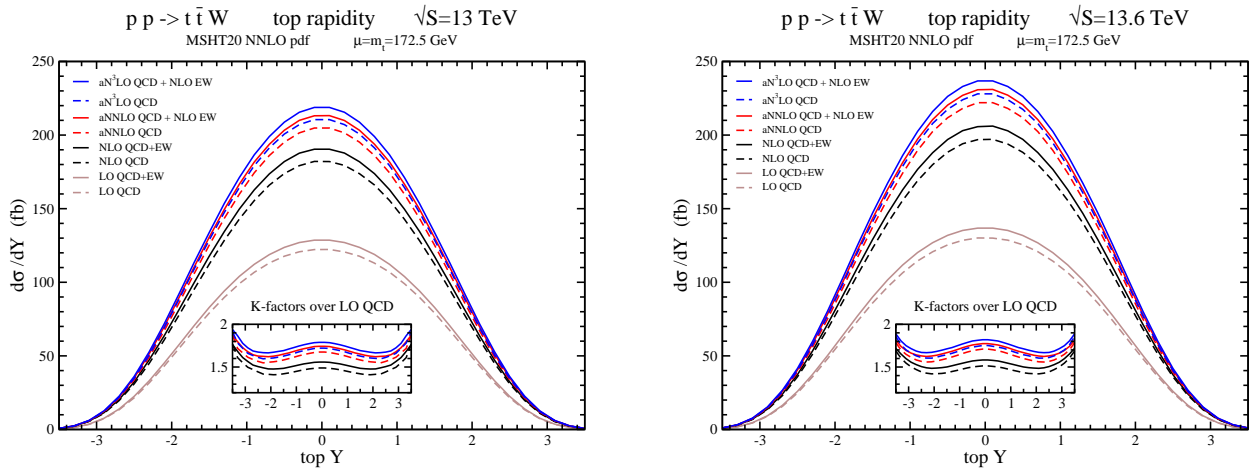


Figure 3: The top-quark rapidity distributions at various orders through aN^3LO QCD + NLO EW in $t\bar{t}W$ production in pp collisions at LHC energies of 13 TeV (left plot) and 13.6 TeV (right plot) using MSHT20 NNLO pdf. The inset plots display the K -factors relative to LO QCD.

5 Conclusions

We have provided a study of higher-order corrections for $t\bar{t}W$ production at the LHC. We have included exact QCD corrections at NLO as well as soft-gluon corrections at aNNLO and aN^3LO . We have also included electroweak corrections through NLO. We have calculated total cross sections as well as top-quark differential distributions for $t\bar{t}W$ production at LHC energies through aN^3LO QCD + NLO EW.

The total cross sections get large enhancements from the complete NLO QCD and electroweak corrections. The additional aNNLO and aN^3LO QCD corrections from soft-gluon emission are significant, accounting for further enhancements of the cross section. The theoretical uncertainties from scale variation get reduced with each increasing perturbative order. We have also provided results separately for $t\bar{t}W^+$ and $t\bar{t}W^-$ production. The aN^3LO corrections are necessary to find agreement with the LHC data at 8 and 13 TeV.

We have also computed the top-quark p_T and rapidity distributions for two recent center-of-mass LHC energies, namely 13 TeV and 13.6 TeV. These differential distributions also receive large QCD corrections at NLO and further significant enhancements at aNNLO and aN^3LO , as well as significant electroweak corrections. The effects of these enhancements depend on the value of the top-quark transverse momentum or rapidity.

Acknowledgements

This material is based upon work supported by the National Science Foundation under Grant No. PHY 2112025.

References

- [1] CMS Collaboration, *Measurement of associated production of vector bosons and top quark-antiquark pairs in pp collisions at $\sqrt{s} = 7$ TeV*, Phys. Rev. Lett. **110**, 172002 (2013) [arXiv:1303.3239].
- [2] CMS Collaboration, *Measurement of the top quark-antiquark pair production in association with a W or Z boson in pp collisions at $\sqrt{s} = 8$ TeV*, Eur. Phys. J. C **74**, 3060 (2014) [arXiv:1406.7830].
- [3] ATLAS Collaboration, *Measurement of the $t\bar{t}W$ and $t\bar{t}Z$ production cross sections in pp collisions at $\sqrt{s} = 8$ TeV with the ATLAS detector*, JHEP **11**, 172 (2015) [arXiv:1509.05276].
- [4] CMS Collaboration, *Observation of top quark pairs produced in association with a vector boson in pp collisions at $\sqrt{s} = 8$ TeV*, JHEP **01**, 096 (2016) [arXiv:1510.01131].
- [5] ATLAS Collaboration, *Measurement of the $t\bar{t}Z$ and $t\bar{t}W$ production cross sections in multilepton final states using 3.2 fb^{-1} of pp collisions at $\sqrt{s} = 13$ TeV with the ATLAS detector*, Eur. Phys. J. C **77**, 40 (2017) [arXiv:1609.01599].
- [6] CMS Collaboration, *Measurement of the cross section for top quark pair production in association with a W or Z boson in proton-proton collisions at $\sqrt{s} = 13$ TeV*, JHEP **08**, 011 (2018) [arXiv:1711.02547].
- [7] ATLAS Collaboration, *Measurement of the $t\bar{t}Z$ and $t\bar{t}W$ cross sections in proton-proton collisions at $\sqrt{s} = 13$ TeV with the ATLAS detector*, Phys. Rev. D **99**, 072009 (2019) [arXiv:1901.03584].
- [8] CMS Collaboration, *Measurement of the cross section of top quark-antiquark pair production in association with a W boson in proton-proton collisions at $\sqrt{s} = 13$ TeV*, JHEP **07**, 219 (2023) [arXiv:2208.06485].
- [9] ATLAS Collaboration, *Measurement of the total and differential cross-sections of $t\bar{t}W$ production in pp collisions at 13 TeV with the ATLAS detector*, ATLAS-CONF-2023-019 (2023).
- [10] S. Badger, J.M. Campbell, and R.K. Ellis, *QCD corrections to the hadronic production of a heavy quark pair and a W -boson including decay correlations*, JHEP **03**, 027 (2011) [arXiv:1011.6647].
- [11] J.M. Campbell and R.K. Ellis, *$t\bar{t}W^\pm$ production and decay at NLO*, JHEP **07**, 052 (2012) [arXiv:1204.5678].
- [12] M.V. Garzelli, A. Kardos, C.G. Papadopoulos, and Z. Trocsanyi, *$t\bar{t}W^\pm$ and $t\bar{t}Z$ hadroproduction at NLO accuracy in QCD with parton shower and hadronization effects*, JHEP **11**, 056 (2012) [arXiv:1208.2665].
- [13] F. Maltoni, D. Pagani, and I. Tsinikos, *Associated production of a top-quark pair with vector bosons at NLO in QCD: impact on $t\bar{t}H$ searches at the LHC*, JHEP **02**, 113 (2016) [arXiv:1507.05640].

- [14] S. Frixione, V. Hirschi, D. Pagani, H.-S. Shao, and M. Zaro, *Electroweak and QCD corrections to top-pair hadroproduction in association with heavy bosons*, JHEP **06**, 184 (2015) [arXiv:1504.03446].
- [15] R. Frederix, D. Pagani, and M. Zaro, *Large NLO corrections in $t\bar{t}W^\pm$ and $t\bar{t}t\bar{t}$ hadroproduction from supposedly subleading EW contributions*, JHEP **02**, 031 (2018) [arXiv:1711.02116].
- [16] L. Buonocore, S. Devoto, M. Grazzini, S. Kallweit, J. Mazzitelli, L. Rottoli, and C. Savoini, *Associated production of a W boson with a top-antitop quark pair: next-to-next-to-leading order QCD predictions for the LHC*, arXiv:2306.16311.
- [17] N. Kidonakis and G. Sterman, *Subleading logarithms in QCD hard scattering*, Phys. Lett. B **387**, 867 (1996).
- [18] N. Kidonakis and G. Sterman, *Resummation for QCD hard scattering*, Nucl. Phys. B **505**, 321 (1997) [arXiv:hep-ph/9705234].
- [19] N. Kidonakis, *Two-loop soft anomalous dimensions and next-to-next-to-leading-logarithm resummation for heavy quark production*, Phys. Rev. Lett. **102**, 232003 (2009) [arXiv:0903.2561].
- [20] N. Kidonakis, *Next-to-next-to-leading soft-gluon corrections for the top quark cross section and transverse momentum distribution*, Phys. Rev. D **82**, 114030 (2010) [arXiv:1009.4935].
- [21] N. Kidonakis, *NNNLO soft-gluon corrections for the top-antitop pair production cross section*, Phys. Rev. D **90**, 014006 (2014) [arXiv:1405.7046].
- [22] N. Kidonakis, *NNNLO soft-gluon corrections for the top-quark p_T and rapidity distributions*, Phys. Rev. D **91**, 031501 (2015) [arXiv:1411.2633].
- [23] N. Kidonakis, M. Guzzi, and A. Tonerio, *Top-quark cross sections and distributions at approximate N^3LO* , Phys. Rev. D **108**, 054012 (2023) [arXiv:2306.06166].
- [24] N. Kidonakis, *Next-to-next-to-leading logarithm resummation for s -channel single top quark production*, Phys. Rev. D **81**, 054028 (2010) [arXiv:1001.5034].
- [25] N. Kidonakis, *Two-loop soft anomalous dimensions for single top quark associated production with a W^- or H^-* , Phys. Rev. D **82**, 054018 (2010) [arXiv:1005.4451].
- [26] N. Kidonakis, *Next-to-next-to-leading-order collinear and soft gluon corrections for t -channel single top quark production*, Phys. Rev. D **83**, 091503 (2011) [arXiv:1103.2792].
- [27] M. Forsslund and N. Kidonakis, *Resummation for $2 \rightarrow n$ processes in single-particle-inclusive kinematics*, Phys. Rev. D **102**, 034006 (2020) [arXiv:2003.09021].
- [28] M. Forsslund and N. Kidonakis, *Soft-gluon corrections for the associated production of a single top quark and a Higgs boson*, Phys. Rev. D **104**, 034024 (2021) [arXiv:2103.01228].
- [29] N. Kidonakis and N. Yamanaka, *QCD corrections in $tq\gamma$ production at hadron colliders*, Eur. Phys. J. C **82**, 670 (2022) [arXiv:2201.12877].
- [30] N. Kidonakis and N. Yamanaka, *Soft-gluon corrections for tqZ production*, Phys. Lett. B **838**, 137708 (2023) [arXiv:2210.09542].

- [31] N. Kidonakis and A. Tonerio, *Higher-order corrections in $t\bar{t}\gamma$ cross sections*, Phys. Rev. D **107**, 034013 (2023) [arXiv:2212.00096].
- [32] H.T. Li, C.S. Li, and S.A. Li, *Renormalization group improved predictions for $t\bar{t}W^\pm$ production at hadron colliders*, Phys. Rev. D **90**, 094009 (2014) [arXiv:1409.1460].
- [33] A. Broggio, A. Ferroglia, G. Ossola, and B.D. Pecjak, *Associated production of a top pair and a W boson at next-to-next-to-leading logarithmic accuracy*, JHEP **09**, 089 (2016) [arXiv:1607.05303].
- [34] A. Kulesza, L. Motyka, D. Schwartzlander, T. Stebel, and V. Theeuwes, *Associated production of a top quark pair with a heavy electroweak gauge boson at NLO+NNLL accuracy*, Eur. Phys. J. C **79**, 249 (2019) [arXiv:1812.08622].
- [35] A. Broggio, A. Ferroglia, R. Frederix, D. Pagani, B.D. Pecjak, and I. Tsinikos, *Top-quark pair hadroproduction in association with a heavy boson at NLO+NNLL including EW corrections*, JHEP **08**, 039 (2019) [arXiv:1907.04343].
- [36] G. Sterman, *Summation of large corrections to short-distance hadronic cross sections*, Nucl. Phys. B **281**, 310 (1987).
- [37] A. Ferroglia, M. Neubert, B.D. Pecjak, and L.L. Yang, *Two-loop divergences of QCD scattering amplitudes with massive partons*, Phys. Rev. Lett. **103**, 201601 (2009) [arXiv:0907.4791].
- [38] N. Kidonakis, *Soft anomalous dimensions and resummation in QCD*, Universe **6**, 165 (2020) [arXiv:2008.09914].
- [39] N. Kidonakis, *Four-loop massive cusp anomalous dimension in QCD: A calculation from asymptotics*, Phys. Rev. D **107**, 054006 (2023) [arXiv:2301.05972].
- [40] J. Alwall *et al.*, *The automated computation of tree-level and next-to-leading order differential cross sections, and their matching to parton shower simulations*, JHEP **07**, 079 (2014) [arXiv:1405.0301].
- [41] R. Frederix, S. Frixione, V. Hirschi, D. Pagani, H.-S. Shao, and M. Zaro, *The automation of next-to-leading order electroweak calculations*, JHEP **07**, 185 (2018) [Erratum: JHEP **11**, 085 (2021)] [arXiv:1804.10017].
- [42] S. Bailey, T. Cridge, L.A. Harland-Lang, A.D. Martin, and R.S. Thorne, *Parton distributions from LHC, HERA, Tevatron and fixed target data: MSHT20 PDFs*, Eur. Phys. J. C **81**, 341 (2021) [arXiv:2012.04684].